Aerodynamic Design of a Land Speed Record Car

T. P. TORDA* AND THOMAS A. MOREL†
Illinois Institute of Technology, Chicago, Ill.

Over-all aerodynamic design considerations of The Blue Flame, a car which holds the world land-speed record, are discussed. Lift, drag, acceleration and deceleration characteristics are presented. Estimated drag coefficients and wind-tunnel results on a $\frac{1}{25}$th scale model are compared with data measured during an actual speed run of The Blue Flame. Actual subsonic drag was found to be slightly lower than predicted.

Introduction

ON October 23, 1970, The Blue Flame experimental car was driven across Utah's Bonneville Salt Flats to a new world land-speed record of 622.407 mph. The Blue Flame is powered by a rocket propulsion system using liquefied natural gas (LNG) for fuel. The fuel is oxidized with hydrogen peroxide. The Blue Flame's engine weights 770 lb and can develop 58,000 hp. The vehicle is 38 ft 2.6 in. long, stands 8 ft 8 in. high at the tail and weighs 6500 lb, dry. It was built by Reaction Dynamics, Inc., of Milwaukee, Wis. T. P. Torda and S. C. Uzgiris of the Illinois Institute of Technology were responsible for the aerodynamics and mechanical design.

Aerodynamic Design Considerations

The aerodynamic shape of The Blue Flame (Figs. 1 and 2) was determined in three phases: preliminary aerodynamic design; wind-tunnel tests; and, final shape determination due to structural and space requirements. During the preliminary design phase, results of some pertinent high-speed sled experiments were used.

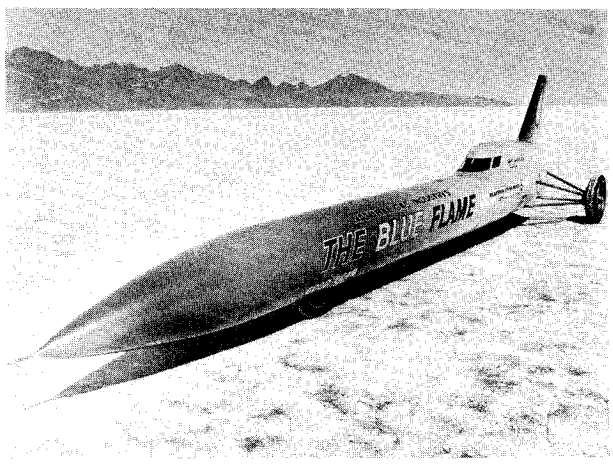

Fig. 1 The Blue Flame on Bonneville salt flats.

Hermann et al.,[1-3] have established that besides its dependence on the angle of attack, the lift coefficient at supersonic speeds varies directly with the square of the fineness ratio, inversely with the nose length (referred to a total body length), and inversely with the height above the ground.

For drag reduction at supersonic speeds, nose shape and fineness ratio are most important. Increasing fineness ratio of the body increases the critical Mach number and decreases the transonic drag rise. Drag may be also influenced by the change of height because flow separation on the lower surface is affected by the pressure distribution and by reflected shocks. Important contributions to the drag of the vehicle come from the interference drag.

As was found in supersonic sled tests,[2] the shocks generated on the nose are reflected from the ground. This changes the pressure distribution and the flow pattern particularly on the lower surfaces. In general, these shock reflections cause a pressure build-up and, at supersonic speeds, a net lift force results which increases in the flow direction. At transonic and low-supersonic speeds, the situation is different and the interaction between the lower surface and ground are less predictable. At subsonic speeds, the ground interference produces a downward lift (or suction)—because the flow between the body and the ground is accelerated.[1,2] In addition, due to compressibility effects, the suction force increases with increasing Mach number.[1,3] In the transonic range, a reversal in the direction of the lift forces occurs. This reversal may be sudden and will cause a change in the angle of attack due to the flexibility of the suspension and of the structure. Finally,on a flat bottom vehicle, choking of the flow under it may occur, causing large lift and drag.[1,5]

Ground interference may be alleviated by: increasing the height of the body above ground; keeping the lower surface parallel to the ground or slightly sloping up in the flow direc-

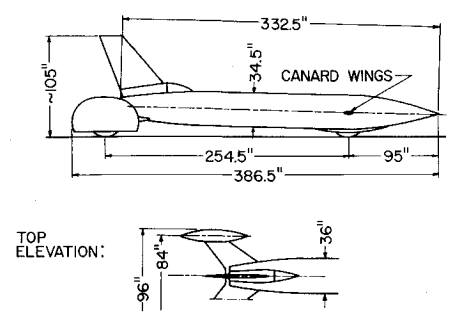

Fig. 2 Outline drawing of The Blue Flame.

Received October 26, 1970; revision received June 7, 1971. The work reported was carried out for partial fulfillment of the requirements for the Degree of Master of Science in Mechanical and Aerospace Engineering under the sponsorship of the American Gas Association (in cooperation with the Institute of Gas Technology and Reaction Dynamics, Inc.).

Index categories: Rocket Vehicle Aerodynamics; Liquid Rocket Engines; and Aerospace Technology Utilization.

* Professor of Mechanical and Aerospace Engineering.

† Graduate Student, Research Fellow in the Mechanical and Aerospace Engineering Dept.

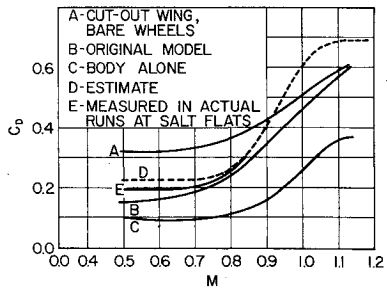

Fig. 3. Drag characteristics.

tion at the rate of boundary-layer build-up; flat bottom should be avoided. The body cross section used has a shape of a rounded-off triangle standing on its tip which promotes cross-flow from the high-pressure area on the bottom to the sides and the top of the body. Such cross-flow reduces the lift. In addition, the body was inclined under a negative angle of attack of approximately $1\frac{1}{2}°$, since a slight negative angle of attack causes large reductions of lift, whereas its effect on drag is not too significant. A small nose droop was incorporated which further decreases the lift forces in the transonic and supersonic regions. These also improved the driver's view, since his seat is located far back between the last tank and the engine to give a better control over steering.

An ogival nose shape was chosen since Stoney[16] has shown that the von Kármán ogive[19,20] has the smallest pressure drag in the transonic region. In order to have better control over lift, a small triangular canard wing is mounted on each side of the nose (NACA 66-series airfoil).

After the critical Mach number (M_{crit}) is exceeded, the value of the drag coefficient rises abruptly. M_{crit} increases with increasing fineness ratio of a body and may be delayed by appropriate design. The magnitude of the transonic drag rise is governed by the rate of axial development of the cross-sectional area which should be slow (area rule).[15] Using the image method, the area rule was applied in this design despite the vicinity of ground.

Friction drag on well streamlined bodies is an important part of the overall drag in the subsonic region, but at transonic and supersonic speeds, the pressure drag will dominate. The flow around the afterbody depends primarily on the shape of the boat-tail, its juncture with the body and, if present, on the effects of a jet issuing from the base.[8–12] Therefore, a parabolic, smoothly faired boat tail was chosen for the afterbody.

The wheels, and mainly the tires, presented one of the main problems in aerodynamic design of the car. Several configurations were studied. First, front and rear track of approximately equal size was chosen (about 70 in.) with the wheels exposed. No information could be found regarding the drag of exposed wheels, as compared to faired ones, but it may be large because of the high-relative velocity of the top of the tires and the blunt shape. The next configuration had a narrower track with the wheels faired into the body. Such a solution would have important disadvantages. The large tire diameter leads to sizable protrusions extending above the top surface of the vehicle causing flow separation and excessive drag. Further, the flat bottom and small height above the ground, inherent in this design, would cause high-ground interference and a dangerous lift force.

In the final design, the two front wheels are imbedded in the car's body. The front track is kept very narrow. This is advantageous from a structural point of view and also for reduction of the frontal area. However, the wake formation behind a double wheel arrangement as compared to weaker wakes behind separated wheels should be investigated. The rear wheels extend behind the body of the car and have a wide track to increase roll stability; the position in the axial direction was determined by the area rule. In the original design, the rear wheels were connected to the body by a wing-like structure. (NACA 66-series profile with a thickness ratio of approximately 13%.) The leading edge of the wing was swept back at an angle of 56° to delay critical drag rise. The wind-tunnel tests have shown adverse influence of wing structure on the pitching moment. Therefore, the horizontal surfaces were eliminated and strut supports were used.

The drag of the rear wheels consists of the drag of the fairings and viscous resistance inside them. Slender fairings were to reduce the pressure drag. The magnitude of viscous resistance inside was estimated to be at most on the order of 10 lb at 800 mph, which is not important.

There are no experimental data available to estimate the pressure inside the wheel fairings and front wheel well at high speeds, and a test of a full-size model in a wind tunnel would be necessary to predict it. There was no opportunity to conduct such tests but the pressure inside of the front wheel well will be monitored during future runs.

Directional stability of the car is very important and has to be ensured at all speeds. This means that the side force center of pressure should be kept behind the center of gravity. Well-streamlined slender bodies have the center of pressure far forward. To balance this and to shift the side force center of pressure back, a vertical fin in the rear is needed.[18] Also, care should be taken to keep the center of gravity of the car as much forward as possible. The tail fin of The Blue Flame is a swept back low-drag NACA 66-008 airfoil.[17]

The cockpit is in the rear and is long and faired in smoothly in order to delay separation. The space in the cockpit fairing behind the driver is used to accommodate two parallel containers each of which contains two braking parachutes. This dictated the shape of the fairing which has a blunt base. One of the parachute sets is designed to be used for braking during the run; the other set is a reserve one.

Estimate of Over-all Drag

The drag estimate was based upon experimental data.[13,14,16,17,19,21] It was obtained as a sum of the drag of all car components at subsonic speeds corrected for estimated contributions of base drag, mutual interference and ground interference. The experimental transonic drag-rise[15,16] was taken as a base for an estimate of the transonic drag coefficient.

Subsonic Drag Coefficient

The subsonic drag coefficient of each component was estimated using the references noted, except that no reference was available for assessing the drag coefficient of rear wheel fairings. This was estimated as $C_D = 0.18$ (see Table 1).

Drag coefficient based on the total frontal area is $C_D = 2.631/15.30 = 0.172$‡, the combined drag is usually larger than the sum of the drag of individual components due to interference drag originating at the joints of components. To reduce interference drag wings or fin should be attached on places where the local velocity is low or where the boundary layer is thick so that the root is not exposed to high flow velocity; the junctures of two different components with the

Table 1 Subsonic drag coefficient

	Reference area	C_D	$A \times C_D$	Frontal area: A
Body	6.95	0.20[16]	1.390	6.95
Wings	23.60	0.004[17]	0.094	1.60
Tail fin	26.40	0.004[17]	0.102	0.95
Fairings	5.80	0.18	1.045	5.80
			2.631	15.30 ft²

‡ The total frontal area was obtained by adding the frontal area of the wheels and that of the cockpit ($A = 18.5$ ft²). From this point on, the total frontal area was used in data reduction.

body should be displaced longitudinally; surfaces should be joined perpendicularly and faired smoothly.

Corrections

The drag coefficient was increased to provide for mutual interference,[15] ground interference and base drag. This increase was based on a study of the subsonic drag coefficient of Craig Breedlove's Spirit of America. First, the drag coefficient of the Spirit of America was estimated using the method described previously. Then an actual over-all drag coefficient was found from known values of thrust and top speed, taking also into account rolling resistance. The ratio of these two coefficients was 1.30. This ratio was used to correct the drag coefficient to $C_D = 0.172 \times 1.30 = 0.23$. Based on the experimentally found transonic drag-rise,[15,16] it was estimated that C_D will triple in the transonic region. The onset of the critical drag-rise was expected already at $M = 0.75$ due to the fact that the area rule could not be applied strictly in the rear of the car. The estimated C_D is shown in Fig. 3 by a broken line. The drag force based on this estimated drag coefficient is in Fig. 4.

Skin Friction and Rolling Resistance

Generally, for well-streamlined bodies, most of the drag at subsonic speeds is skin-friction drag whereas at transonic speeds the pressure drag predominates. The skin-friction drag was computed as a sum of contributions over all parts of the vehicle. The skin-friction coefficient was corrected for the compressibility effects and it was found that at 750 mph ($M = 1$) the skin friction will form approximately 15% of the over-all drag.

The rolling resistance in per cent of the total download was computed according to Hoerner[13] $K_r(\%) = 0.5 + 15/p + 0.0035V^2/p$ where p is a tire pressure in psia and V velocity in mph. The formula was modified to account for the flexibility of the ground by taking $p = 100$ psia only (instead of the actual tire pressure of 300 psi).

Acceleration and Deceleration

For an estimate of acceleration and deceleration, the equation of motion with variable mass was solved to determine the maximum speed, average speed and the length of track needed for acceleration. The expected performance was computed based on the following data: estimates of the aerodynamic drag and rolling resistance, thrust of 22,000 lb, fuel burning time 20 sec and starting weight of the car 6000 lb. The results are presented in Fig. 5.

The results of the computations show that the run should be started at a distance of 8850 ft from the beginning of the measured mile and that the average speed in the measured mile will then be 817 mph ($M = 1.09$). Further, a gradual shut-off of the engine will be necessary to avoid large decelerations arising in case the shut-off is abrupt. The expected

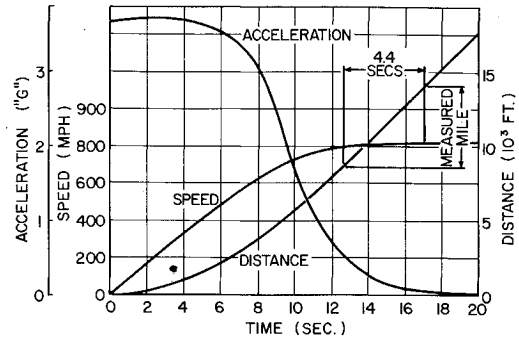

Fig. 5 Acceleration phase.

deceleration of the car is indicated in Fig. 6. The drag decreases fast with the speed so that the engine may be completely shut off below 700 mph. The car will then coast to 600 mph when the first parachute opens and later a second one will be used. The disc brakes will be applied at a speed of 150 mph. The distance over which the vehicle will decelerate to a full stop is not to exceed three miles to leave some safety margin on the ten-mile track in Bonneville.

Wind-Tunnel Tests

Wind-tunnel tests were carried out to determine ground interference effects (lift and pitching moment); drag of the vehicle as a check on the original estimate; the validity of the area rule in close proximity to the ground; lateral characteristics, especially the position of the side-force center of pressure; and, the performance of several different configurations: e.g., canard wings, drooped nose, etc.

The wind-tunnel tests were conducted under the supervision of J. D. Lee, Director of the Transonic Wind Tunnel Laboratory at Ohio State University, Columbus, Ohio. The tunnel has 12 × 12-in. perforated-wall test section and its Mach number range is up to $M = 1.5$.

The model for the wind-tunnel tests was a 1:25 scale and was suspended in the test section by a sting support simulating the engine jet. The ground effect was simulated by mounting the model above a ground plate. The condition of the turbulent boundary layer along the plate was monitored by 15 pressure taps to determine presence of separation. The boundary layer on the model was tripped by a transition strip located on the nose. The tests were conducted in a Mach number range from 0.5 to 1.15.

To check the testing procedures, various components of the model were removed or added, and consistency of the obtained results was examined. Also, results of tests performed close to, or away from the ground plate were correlated and it was concluded that the simulation was adequate for scaling purposes. The model was tested at 0° and −1.25°.

Drag characteristics for different configurations are on Fig. 3. In the subsonic region C_D of the second configuration

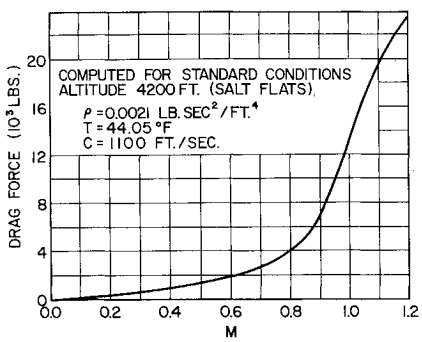

Fig. 4 Drag force.

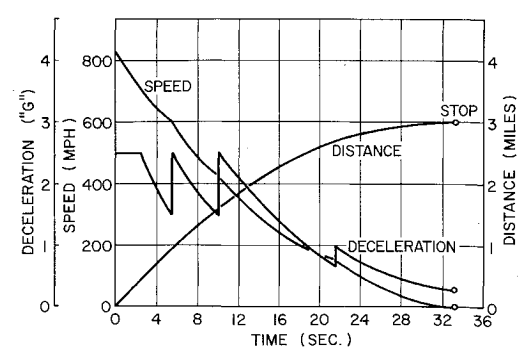

Fig. 6 Decleration phase.

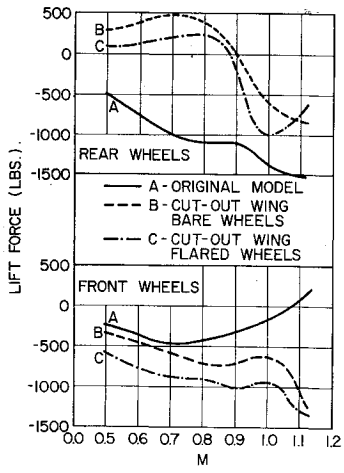

Fig. 7 Lift force.

(with cut-out wings and bare wheels) is much larger than C_D of the original model; in the transonic region, however, there is much smaller rise of the drag coefficient which compensates for the large subsonic value. The test results seem to confirm the validity of the area rule in the vicinity of the ground. The second configuration has a more favorable cross-sectional area distribution than the original design due to the substantial reduction of the cross-sectional area of the rear wheel suspension. Note that the transonic drag increment of this configuration ($\Delta C_D = 0.30$) is close to the one of the body alone ($\Delta C_D = 0.28$), whereas the transonic drag increment on the original design is made larger and exceeds 0.45; which is what the area rule suggests.

Lift and pitching moment characteristics were measured on three configurations: the original model with the wing and faired wheels, and two configurations with the cut-out wing, one with bare rear wheels and one with rear wheel fairings. In all three cases the body was at a negative angle of attack of $-1.25°$. The lift and the pitching moment were reduced into two normal forces, one acting at the front wheels and the second at the rear wheels (Fig. 7).

The tests have shown a tendency towards a positive lift on the front part of the model. It was determined that the wing-like structure which supported the rear wheels was the source of lift forces and its replacement by struts was considered. Because of that, the configuration with cut-out wings (simulating struts) was incorporated into the test program. The improvement achieved by elimination of the wing can be seen in Fig. 7. It was on the basis of this evidence that the decision was made in favor of the struts despite the large increase in subsonic drag coefficient which it causes. It is clearly necessary to avoid any danger of lifting of the front wheels off the ground. The tests revealed a strong influence of the front wheels on the lift and pitching moment characteristics due to a strong wake formed behind the front wheels which interferes with the wing. Measurements of pressure distribution along the ground plate indicate that only local separation of the boundary layer on the plate occurred. Therefore, a similar effect to that measured can be expected during an actual run.

Lateral characteristics of the model (position of the side-force center of pressure and a side force coefficient) have shown that the car will have sufficient directional stability and, therefore, the tail fin was kept in the same form as designed. The influence of the triangular canard wings located at the front wheels, have also been investigated. The results showed their effectiveness and canard wings were used on the car.

Instrumentation

The performance of the car has to be monitored to avoid critical situations. After every run an analysis must be made of handling, stability, aerodynamic loads and engine performance, as well as the dynamic behavior of the structure, especially of the little damped rear assembly. Besides the cockpit instruments, the car is equipped with two 12-channel recording galvanometers monitoring pressure transducers, strain gages, horizontal and vertical accelerometers and an engine thermocouple.

The pressure transducers were placed along the length of the body on its top, bottom, sides and also at the base. Other transducers were on the top and the side of the front wheel cover which is sealing off the wheel well to protect the interior of the car from salt. There is no information whether there is a pressure buildup or a depression inside a wheel housing due to the viscous pumping of the wheels at high speeds.

The ultimate speed of the car was to be achieved stepwise and the amount of fuel loaded into the car was reduced for the slower runs. After each of the runs, the recorded data, together with the personal account of the driver were analyzed. If no critical trend appeared in the data, then a higher speed run followed; otherwise necessary adjustments had to be made first.

Unfortunately, the pressure readings obtained are small since sufficiently sensitive pressure transducers or high quality recording equipment were not available. Meaningful readings would be obtained with the present equipment only at speeds higher than Mach number of unity.

The readings of the accelerometer were integrated after each run by a numerical-graphical procedure to obtain the velocity and distance as a function of time. The thrust of the engine was then evaluated from the burning rates and of variation of the drag with velocity. The magnitude of the drag was estimated from the deceleration of the car after the burn-out. It was found that the subsonic drag coefficient is lower than predicted; see curve *e* of Fig. 3.

As far as the aerodynamic loads are concerned, the driver reported no discernible trend toward lifting or dipping of the car's front. The directional stability has been excellent and small deviations from the straight course were corrected by steering of the front wheels.

References

[1] Hermann, R., Melnik, W. and Moynihan, F., "Aerodynamic Investigation of Sled Configurations for the Holloman Track," AFMDC-TR-59-18 June 1959, Holloman Air Force Base, N. M.

[2] Hermann, R., Moynihan, F., and Peterson, H., "Experimental Aerodynamic Investigation of Basic Rocket Sled Configurations, M = 1.5 to M = 3.0," Research Rept. No. 167, also AFMDC-TR-59-41, Oct. 1959, Rosemount Aeronautical Laboratories, Institute of Technology, Univ. of Minnesota, Minneapolis, Minn.

[3] Hermann, R. and Melnik, W. L., "Approximate Theory of Ground Interference on Slender Rocket Sleds of Arbitrary Cross-Section with Application to the Configuration Rocketdyne RS-2 Sled," AFMDC-TR-60-1, Jan. 1960, Holloman Air Force Base, N. Mex.

[4] Wimbrow, William R., "Wind Tunnel Testing of High Speed Track Sleds," Oct. 1958, Propulsion Wind Tunnel Facility, ARO, Inc.,

[5] Ankeney, D. P., "Comparison of Experimental and Theoretical Pressure Distribution Caused Ground Interference Effects on Horizontal-Wedge Test-Track Sleds," NOTS TP 2533, NAVWEPS Rept. 7564, Aug. 15, 1960, U. S. Naval Ordnance Test Station, China Lake, Calif.

[6] Wu, T. Y., "Ground Interference Effects on Bodies Moving through a Compressible Fluid and Their Application to SNORT Sled Designs," NOTS 2118, NAVORD Rept. 6420, July 1, 1958, U. S. Naval Ordnance Test Station, China Lake, Calif.

[7] "Supersonic Tracks" NOTX 1938, Rev. 1, Sept., 1962, U. S. Naval Ordnance Test Station, China Lake, Calif.

[8] Shrewsbury, G. D., "Effect of Boat-Tail Juncture Shape on Pressure Drag Coefficient of Isolated Afterbodies," TM-X-1517, March 1968, NASA.

[9] Bowman, J. E. and Clayden, W. A., "Boat-Tailed Afterbodies at M = 2 with Gas Ejection," *AIAA Journal*, Vol. 6, No. 10, Oct. 1968, pp. 2029–2030.

[10] Cortright, E. M., Jr. and Kochendorfer, F. D., "Jet Effects on Flow Over Afterbodies in Supersonic Stream," RM-E53H25, NACA.

[11] Beheim, M. A., Klann, J. L., and Yeager, R. A., "Jet Effects on Annular Base Pressure and Temperature in a Supersonic Stream," TR R-125, 1962, NASA.

[12] Compton, W. B., III, "Effect on Base Drag of Recessing the Bases of Conical Afterbodies at Transonic and Supersonic Speeds," TN D-4821, Oct. 1968, NASA.

[13] Hoerner, S. F., "Fluid-Dynamic Drag," published by the author, 1965, Midland Pk., N. J.

[14] Hoerner, S. F., "Compressibility Effects on Drag," TR F-TR-1188-IA, ATI No. 43187, Central Air Documents Office.

[15] Whitcomb, R. T., "A Study of the Zero-Lift Drag-Rise Characteristics of Wing-Body Combinations Near the Speed of Sound," Rept. 1273, 1956, NACA.

[16] Stoney, W. E., "Collection of Zero-Lift Data on Bodies of Revolution from Free-Flight Investigations," TN 4201, Jan. 1958, NACA.

[17] Abott, I. H., von Doenhoff, A. E., and Stivers, L. S., Jr., "Summary of Airfoil Data." Rept. 824, 1945, NACA.

[18] DeJonge, C., "The Effect of Low Ratio Rectangular and Delta Cruciform Fins on the Stability of Bodies of Revolution with Tangent Ogives at Small Angles of Attack through a Mach Number Range of 0 to 3.5," RF-TR-62-1, May 23, 1962, U. S. Army Ordnance Missile Command,

[19] Bonney, E. A., *Engineering Supersonic Aerodynamics*, McGraw-Hill, New York, 1950, p. 187.

[20] Nielsen, J., *Missile Aerodynamics*, 1st ed., McGraw-Hill, 1960, p. 284.

[21] Ashley, H. and Landahl, M. T., *Aerodynamics of Wings and Bodies*, Addison-Wesley Reading, Mass., 1965.